WPSA-CPR(17) 17555

X Luo et al.

Assessment of the JT-60SA Divertor Cryopump Performance

Preprint of Paper to be submitted for publication in Proceeding of 13th International Symposium on Fusion Nuclear Technology (ISFNT)

This work has been carried out within the framework of the EUROfusion Consortium and has received funding from the Euratom research and training programme 2014-2018 under grant agreement No 633053. The views and opinions expressed herein do not necessarily reflect those of the European Commission.

This document is intended for publication in the open literature. It is made available on the clear understanding that it may not be further circulated and extracts or references may not be published prior to publication of the original when applicable, or without the consent of the Publications Officer, EUROfusion Programme Management Unit, Culham Science Centre, Abingdon, Oxon, OX14 3DB, UK or e-mail Publications.Officer@euro-fusion.org

Enquiries about Copyright and reproduction should be addressed to the Publications Officer, EUROfusion Programme Management Unit, Culham Science Centre, Abingdon, Oxon, OX14 3DB, UK or e-mail Publications.Officer@euro-fusion.org

The contents of this preprint and all other EUROfusion Preprints, Reports and Conference Papers are available to view online free at http://www.euro-fusionscipub.org. This site has full search facilities and e-mail alert options. In the JET specific papers the diagrams contained within the PDFs on this site are hyperlinked

Assessment of the JT-60SA Divertor Cryopump Performance

Xueli Luo[a], Matthieu Scannapiego[a], Christian Day[a], Shinji Sakurai[b]

[a] *Karlsruhe Institute of Technology, Institute for Technical Physics, 76021 Karlsruhe, Germany*
[b] *National Institutes for Quantum and Radiological Science and Technology, Naka, Ibaraki, 311-0193, Japan*

The cryogenic pumping system is one of the key components that define the operational window of JT-60SA. It is envisaged to utilize condensation pumps that work at 3.8 K, and proper thermal shields cooled with water and 80 K gaseous helium are necessary to allow having them installed at short distance to the torus in order to exploit high pumping speeds. In this paper, one complete divertor cryopump module in a 40° sector is studied by Monte Carlo simulation. The pumping speeds of one cryopump unit for D_2 were found to be between 14.8 m^3/s and 18.1 m^3/s depending on the assumptions taken. In addition, the heat loads to the cryopump condensation pipes during steady state nominal operation, as well as the heat loads and transient behavior after massive gas injection events are assessed. The present design can fulfil the requirement of pumping, cooling and regeneration.

Keywords: cryogenic condensation pump; pumping speed; heat load; test particle Monte Carlo simulation

1. Introduction

The project mission of JT-60SA is to contribute to the early realization of fusion energy by supporting the exploitation of ITER and by complementing ITER in resolving key physics and engineering issues for DEMO reactors [1]. Currently, the machine construction is ongoing within Japanese national funding sources and the Broader Approach between Europe and Japan. A joint research task within the European activities is to support the design of the vacuum systems of JT-60SA, coordinated under the EUROfusion Work Package SA. The main goal of the task is to assess the pumping performances and the cryogenic heat loads of the current design and check that they are in line with the requirements.

The cryogenic pumping system is one of the key components that define the operational window of JT-60SA. It is foreseen that nine cryogenic pumps will be built and installed underneath the divertor. They are cryogenic condensation pumps working at 3.8 K, and proper thermal shields cooled with water and 80 K gaseous helium are necessary to allow having the pumps installed at short distance to the torus in order to exploit high pumping speeds. There are three cryolines which supply two, three and four cryopump units, respectively. This configuration allows for different operational modes in order to vary the effective pumping speed of the complete system. In this paper, a Monte Carlo simulation of the vacuum flow in one 40° sector of the cryopump underneath the divertor cassettes will be presented. The work has been performed with ProVac3D [2-4], a versatile in-house Test Particle Monte Carlo (TPMC) simulation code developed at Karlsruhe Institute of Technology (KIT). Not only the pumping speeds of the pump for different gas species under different boundary conditions and working scenarios were derived, but also the heat loads to the cryopump condensation pipes during steady state nominal operation, and the heat loads and transient behavior after massive gas injection events were assessed.

2. Monte Carlo simulation of one complete cryogenic pump

2.1 Simplified simulation model

According to the current design, the cryopump of JT-60SA is a very complex system underneath the divertor as shown in Fig. 1.

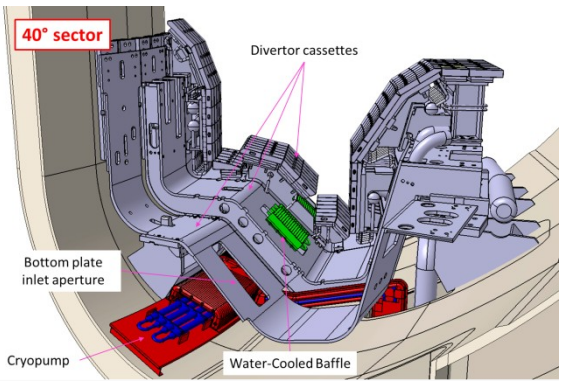

Fig. 1. 40°sector of the JT-60SA divertor pumping system. There are nine independent cryopumps.

In the previous works [5-7], the flow field in the sub-divertor region has been investigated in a simplified 2D domain by means of different Monte Carlo codes, both without and with intermolecular collisions. The goal was to calculate the transmission probability, the Knudsen number, the velocity profiles, and the pressure and temperature distributions. As shown in Fig. 2, the ProVac3D computational domain in this paper follows the contour of the bottom part of the divertor cassette on its upper part down to the vacuum vessel contour on its bottom part. The cryopump domain inlet indicated in Fig. 2 is the interface with the outlet boundary of the sub-divertor neutral gas flow calculation 2D domain. Actually, each of the 40° sector includes four inlet apertures (1 per cassette) in poloidal direction, where the test particles are generated. The surfaces of the condensation pipes are considered as particle sink at which the pumping effect happens.

author's email: Xueli.Luo@kit.edu

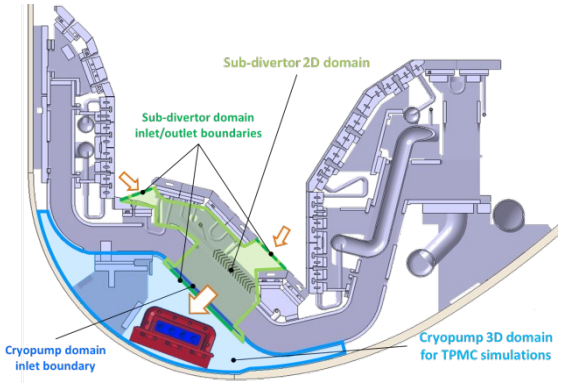

Fig. 2. Sub-divertor and cryopump simulation domains.

One cryopump module of JT-60SA is corresponding to a 40° sector, and two half parts of it (corresponding to a 20° sector) are mirror symmetrical at the center. For simplicity of calculation, the 40° region in Fig. 1 and Fig. 2 is straightened into the simulation domain, and the two toroidal sides of the domain are assumed as periodical boundaries. In this way, the simulation represents one complete cryopump sitting in the real working surroundings of the torus. Fig. 3 shows the PoVac3D geometry of one half sector (20°). Because of the relatively low pressures close to the cryopump, the TPMC simulation approach without consideration of the inter-molecular collisions is eligible. Note that the pumping speed calculated in free molecular regime is conservative, and is expected to increase in the transitional flow regime.

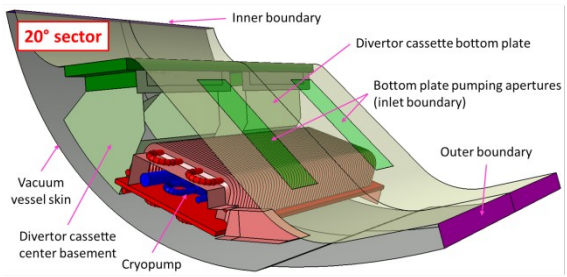

Fig. 3. ProVac3D simulation domain (20° sector).

In the first step, a simplified simulation model was considered, in which the chevron thermal shields was replaced by a box surrounding the condensation pipes. As shown in Fig. 4, three virtual surfaces of the box to mimic the baffle were assumed with an estimated transmission probability of w = 0.27 [8], three other surfaces were closed.

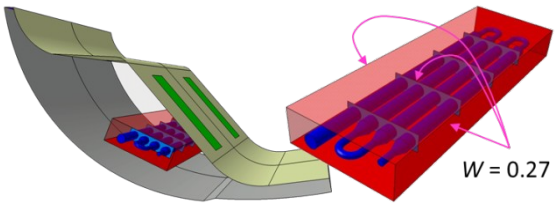

Fig. 4. Simplified simulation domain (20° sector).

author's email: Xueli.Luo@kit.edu

Deuterium molecules at 300 K were generated as test particles at the four pumping apertures. Sticking coefficients (α) in the expected order for H_2/D_2 condensation pumping were applied on the surfaces of the condensation pipes and for the two extreme cases on the inner and outer boundaries to simulate molecules eventually trapped at the far ends of the domain. All simulations were carried out with 10^{11} deuterium molecules in total in the supercomputer Marconi with 1000 CPUs in parallel. Four different cases were considered. The input parameters and the simulation results are summarized in Table 1 and Table 2.

Table 1. Input parameters of four simulation cases.

	Case 1	Case 2	Case 3	Case 4
T of gas at the inlet (K)	300	300	300	300
T of thermal shields (K)	80	80	80	80
T of condensation pipes (K)	3.8	3.8	3.8	3.8
α of condensation pipes	1	1	0.8	0.8
α of inner and outer ends	1	0	1	0

Table 2. Simulation results of the simplified model.

	Case 1	Case 2	Case 3	Case 4
Capture coeff. of two ends	0.15	0	0.15	0
Capture coeff. of cryopump	0.41	0.47	0.39	0.45
Pumping speed (m^3/s)	17.7	20.6	16.8	19.7
For nine cryopumps (m^3/s)	159	185	151	177

The pumping speed S of the cryopump in the table was calculated from the simulated capture coefficient P of the cryopump on the condensation pipes by equation:

$$S=\frac{1}{4}v\cdot A\cdot P, \tag{1}$$

where v is the thermal speed of D_2 molecules at the inlet; A the total area of the four inlet apertures. From the simulation results it can be seen that a reduction of the sticking coefficient from 100% to 80% only reduces the pumping speed by 4-5%. Between a full reflection and a complete trapping of the particles at the inner and outer far ends of the domain, a reduction by 14-15% of the pumping speed was observed.

2.2 Complete simulation model

As shown in Fig. 5, the cyropump has sophisticated chevron thermal shields at 80 K to protect the cryogenic condensations pipes at 3.8 K. For simplicity of calculation, the thermal shields were modeled as surfaces without thickness so that one chevron is comprised of six planes and four ¼ cones. There are 126 chevron baffles in total and the opening distances between the adjacent chevrons were kept at the real value of 10.15 mm in the design. Only this thermal shielding system alone contributed already 1260 components. The simulation was carried out step by step to guarantee the correctness of the simulation of this complex system.

Fig. 5 shows the 80 K supply pipes above and under the base plate. The 80 K baffle pipes above the base plate are integrated into the thermal shielding system. The difficulty here is to simulate the curved connections of two adjacent pipes. Actually, one connection is ½ of one

torus. However, there is no analytical solution of the toroidal surface because it is described by a quartic equation. In order to model it, one curved connection is simplified into nine segments, and each segment is a cylinder of 20 degrees in toroidal direction. Because there are six connections for the condensation pipes and twenty connections for the 80 K supply pipes, they contributed 234 cylinders in the simulation model.

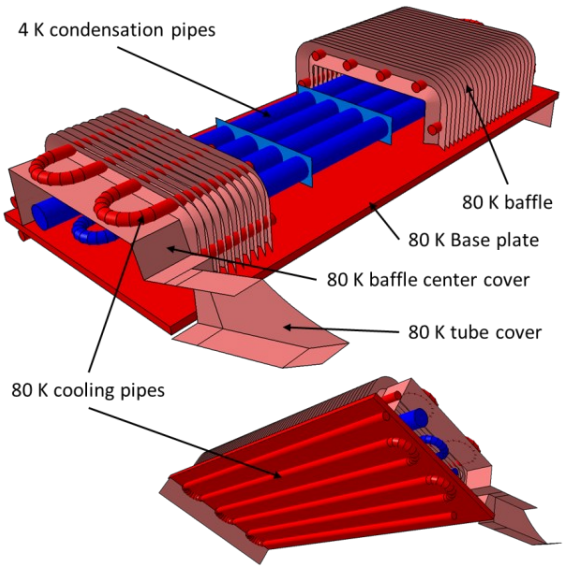

Fig. 5. ProVac3D cryopump model (20° sector).

The complete simulation model also included the center basement, and other auxiliary components such as 80 K baffle center cover and 80 K tube cover. The final model was comprised of 1767 components. Please note that three virtual surfaces were kept, but moved on the tops of the thermal shields in front, inner and outer directions. These virtual surfaces were used to record the local transmission probabilities of the baffles. For this purpose, unlike in the simplified model, they were transparent and had no predefined transmission probability.

Because it is a huge system, we used 6400 CPUs in supercomputer Marconi to simulate 10^{10} test molecules, which delivered sufficient simulation precision. The simulation results are summarized in Table 3.

Table 3. Simulation results of the complete model.

	Case 1	Case 2	Case 3	Case 4
Capture coeff. of two ends	0.15	0	0.15	0
Capture coeff. of cryopump	0.36	0.42	0.34	0.40
Pumping speed (m^3/s)	15.5	18.1	14.8	17.4
For nine cryopumps (m^3/s)	139	163	133	157
Effective pumping speed (m^3/s)	87	96	85	93

We can see that the corresponding pumping speeds are reduced about 12% in all cases. This is because of the blocking effects of the 80 K baffle pipes integrated in the chevron baffles. The last line indicates the effective pumping speed in front of the water-cooled baffle, at an intake temperature of 300 K. These values are slightly lower as the maximum required pumping speed of 100 m^3/s found in the PID [9], but of the same order of magnitude, which is a very good agreement at this design stage. As the capacity of condensation pumps is high, the operative limit of maximum pumped amounts is given by the safety requirement to avoid reliably any oxy-hydrogen explosion hazard in case of an air leak. The design capacity target of 50 000 Pa·m³ [1] is well below the hydrogen inventory safety limit of 10^6 Pa·m³. For the given volume of the vacuum vessel of about 350 m³, this represents a concentration of less than 3 % and, hence, ensures to stay below the lower explosion limit of 5% (D_2 in air at ambient conditions).

Table 4 shows the local transmission probabilities w of the thermal shields, which is defined as

$$w = 1 - \frac{N_2}{N_1}, \qquad (2)$$

where N_1 and N_2 are the numbers of the test molecules entering and exiting the local virtual surfaces of the baffle, respectively.

Table 4. Local transmission probability.

	Case 1	Case 2	Case 3	Case 4
Outer side of thermal shields	0.131	0.147	0.120	0.137
Inner side of thermal shields	0.124	0.133	0.114	0.123
Top side of thermal shields	0.196	0.190	0.186	0.180

It can be seen that the local transmission probability of the thermal shields is influenced by the system geometry and the sticking coefficient of the condensation pipes. It decreases reasonably with smaller values of the sticking coefficient. The values for the inner and outer sides are smaller than the values for the top side. Moreover, for the top side of the chevron baffle, $w = 0.27$ used in the simplified model is about 30% bigger than the accurate value obtained here with the complete model.

Please note that the calculated pumping speeds hold only for pure hydrogenic condensation pumping. It is foreseen to provide helium pumping by means of Ar frost. In this case, the sticking coefficient at the pumping pipes is reduced to α=0.6 [10]. If one further considers 50% coverage of Ar frost on the available cold surfaces, the case is approx. equivalent to α=0.3 with full coverage. The corresponding simulation showed a pumping speed for He of only 11.3 m^3/s for one cryopump unit, or 102 m^3/s for the complete pumping system, respectively, and correspondingly less for the effective pumping speed. In view of the limited pumping capacity of Ar frost for helium, the significant amounts of Ar needed (of the order of 30 times the He amount to be pumped), and the complexity of operation to achieve stable pumping [11, 12], Ar frost pumping is seen critical, in particular for the long pulse and high density scenarios that shall be explored in JT-60SA.

3. Heat load to the cryopump and consequences of MGI on the cryopump operation

Rapid and massive injection of gas particles (MGI) into the plasma is one of a variety of different proposed concepts to safely terminate disrupting plasma for

author's email: Xueli.Luo@kit.edu

machine protection. After a MGI event, the heat fluxes to the cryopump increase and the foreseen injected quantities of material may be large enough to have significant implications on the operation of the divertor pumping system. The saturated vapor temperature for H_2 and D_2 are close to the cryopump nominal operation conditions. If the temperature of the condensation surfaces increase above the saturation temperature, the pump might go into spontaneous regeneration, releasing the gas previously accumulated into the vacuum vessel. Therefore, a parameter study in order to find the operational limits of the existing divertor pumping system has been performed.

3.2 Thermal-hydraulic code despription

For this purpose, a thermal-hydraulic code that works in both steady state nominal pumping operations and transient state has been developed. It is based on code previously developed for a similar assessment of the MGI in ITER [13] that was re-worked for the JT-60SA pumping system. The typical fueling rate in JT-60SA is about 100 Pa·m³/s at a divertor pressure of about few Pa. At an event which triggers MGI, the gas will be injected in few ms, and the pressure at the divertor will suddenly jump. In these transient conditions, the gas throughput from the vacuum vessel to the cryopump is not conserved and is driven by the pressure difference between the different locations. The following outputs are calculated with the code:

- Gas throughput, pressure and temperature upstream the divertor water-baffle, upstream the 80 K inlet baffle, and upstream the 4 K condensation pipes.
- Heat loads to the 4 K condensation pipes: via thermal radiation, solid conduction, nuclear neutron radiation, gas conduction, thermalisation of the gas on the pipes, heat of desublimation, and solid ice cooling on the pipes
- Heat transfer between the 4 K condensation stainless steel pipes and the cryogenic helium flow, 4 K condensation pipes temperature, helium bulk and outlet temperatures and heat load transferred by the cryogenic helium flow

Note that the heat loads to the 80 K thermal shield and baffle and to the 80 K helium coolant have not been studied. The thermal shield system is much heavier and the stainless steel heat capacity at 80 K is much larger than at 4 K, and as a consequence, the temperature of the thermal shield/baffle system is not expected to vary significantly. The thermal radiation and solid conduction heat loads have not been recalculated but taken from the PID document [8] and considered constant during the transient phase following a MGI event. The nuclear neutron radiation heat load is based on the value of 15 mW/cm³ used in a previous analysis of the cryopump [14].

As the type of gas to be injected is still under discussion, calculations for H_2, D_2, Ne and Ar MGI have been performed. With regard to the injected amounts, 400 Pam³ at 300 K is the reference value (scaled from JET), but we varied up to 4000 Pam³, the latter is of the order of the explosion limit if the injected gas would be hydrogenic. After MGI both MGI gas and the gas previously pumped in nominal operation are treated. The thermophysical properties of the gases and from the helium coolant have been calculated or collected from various software and textbooks [15-17]. Some reference input parameters have been defined for the MGI simulations: cryogenic supply helium mass flow of 270 g/s [9], gas temperature upstream the divertor water-cooled baffles of 420 K, gas temperature of 323 K upstream the cryopump 80K inlet baffles and gas temperature of 90 K upstream the cryopump 4 K pipes correspond. The gas temperatures are the maximum expected temperatures in those areas and are thus conservative values.

3.3 Results

In the following graphs, the conditions under nominal D_2 pumping operation are plotted over 5 seconds (-5 to 0), and then the MGI events occur at t = 0. The total heat load under nominal pumping operation at gas throughput of 100 Pa·m³/s is for 305 W for H_2 pumping and 346 W for D_2 pumping. Fig. 6 and Fig. 7 illustrate the influence of the MGI gas amount injected (for D_2 MGI) and the influence of the MGI gas used respectively (at MGI of 4000 Pa·m³).

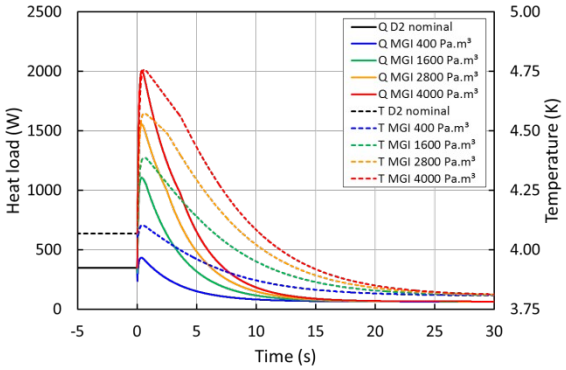

Fig. 6. Total heat load and cryopump condensation pipes temperature evolution after D2 MGI for four different MGI gas amounts.

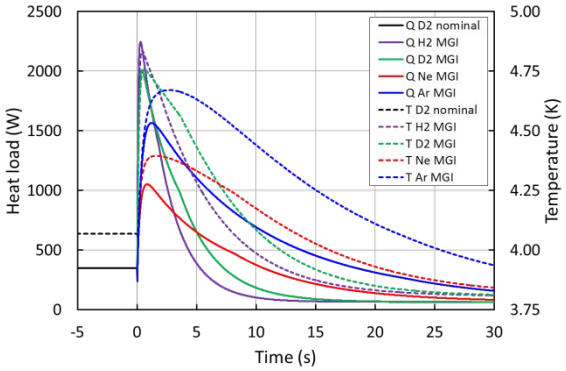

Fig. 7. Total heat load and cryopump condensation pipes temperature evolution after H_2, D_2, Ne and Ar MGI of 4000 Pa·m³.

author's email: Xueli.Luo@kit.edu

The increased pressure and throughput after MGI is accompanied by very large heat loads to the cryopump, increasing the temperature of the condensation pipes very rapidly. This is explained by the fact that the heat capacity of stainless steel at 4 K is very low. Nevertheless, in all calculated cases, the cryopump could recover to normal operation quickly after a MGI event and did not get into spontaneous regeneration. Even under the worst cases, regular pumping was provided again after 50 s, although in the first few seconds after the gas injection, heat loads to the pump were increased up to factor 4.

Note that the nuclear neutron radiation has the highest contribution to the total heat load to the condensation pipes during the nominal pumping steady state operation, but after a MGI event the plasma is killed and this value was considered to be 0. Therefore, the heat load is always dropping down just after the MGI event, but shortly after the high quantity of gas to process results in higher heat loads than in nominal operation.

Fig. 8 illustrates the difference in the temperature evolution of the condensation pipes and the helium coolant after D_2 MGI, with the reference inputs of Table. 3, but with an injected amount of 4000 Pa·m³.

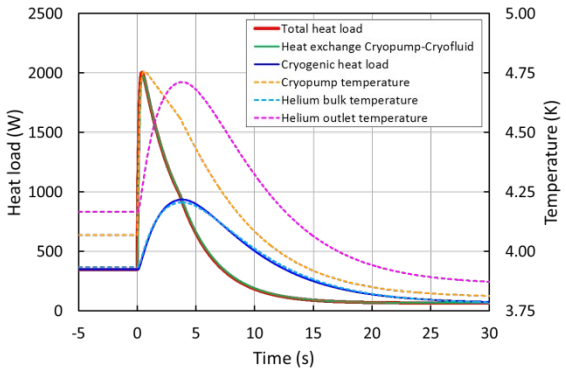

Fig. 8. Heat loads, cryopump condensation pipes temperature, and helium coolant temperature evolution after D_2 MGI of 4000 Pa·m³.

The heat transfer between the helium coolant and the condensation pipes (green curve) is following very closely the total heat load to the condensation pipes. This can be explained by the very fast temperature difference increase between the condensation pipes and the helium coolant (explained by the low heat capacity of stainless steel at 4 K). Therefore, the heat transfer which is directly proportional to the temperature difference between the fluid and the pipe is also promptly varying. On the other hand, the helium mass inventory in the condensation pipes volume has a certain heat capacity that will smooth the heat load transferred by the coolant over the time.

4. Conclusions

The performance of the cryopump of JT-60SA has been thoroughly studied. The pumping speeds under different boundary conditions have been obtained by TPMC simulations. The simulation model is comprised of 1767 components, and can very well represent the complete cryopump in the actual design. The operational window of the pump has been assessed by four bounding cases, and the pumping speeds of one cryopump unit were found to be between 14.8 m^3/s and 18.1 m^3/s. Of course, taking into account the limited conductance of the pumping duct, the effective pumping speeds in front of the water-cooled baffle will decrease, though the found values are close to the requirement of 100 m^3/s (between 85 and 96 m^3/s). Moreover, the local transmission probabilities of the chevron thermal shields and the capture coefficients of four inlet apertures were obtained. The information is useful to the further design works and the simulations of the sub-divertor region.

As next step, it is planned to develop an alternative design based on cryosorption pumping which is able to provide helium pumping speeds in the same order than for hydrogen at extended pumped helium amounts compared to the Ar frost technology. Furthermore, cryosorption pumping of hydrogen is significantly less sensitive to fluctuations of the temperatures of the pumping surfaces than condensation. This would give JT-60SA the capability to also deliver a strong helium programme in support of the early phases of ITER. A thermal-hydraulic code that works in both steady state nominal pumping operations and transient state has been developed and used in the parameter study of the heat loads in order to find the operational limits of the existing divertor pumping system. It is found that the cryogenic performances are in line with the requirements and the design margin before the cryopump goes into regeneration after a MGI event is sufficient.

Acknowledgments

This work has been carried out within the framework of the EUROfusion Consortium and has received funding from the EURATOM research and training programme 2014-2018 under grant agreement No 633053. This work was supported by the EUROFusion HPC project VAC_ND with the resources of supercomputer Marconi-Fusion at CINECA in Italy. The views and opinions expressed herein do not necessarily reflect those of the European Commission.

The authors gratefully acknowledge members of the JT-60SA Integrated Project Team for data exchange and fruitful discussions.

References

[1] JT-60SA Research Unit, JT-60SA Research Plan 2016, www.jt60sa.org/pdfs/JT-60SA_Res_Plan.pdf, v3.3

[2] X. Luo, Chr. Day, Fusion Engineering Design 85 (2010) 1446-1450.

[3] X. Luo, Chr. Day, H. Haas, J. Vac. Sci. Technol. A 29 (2011) 041601.

[4] X. Luo, V. Hauer, Chr. Day, Fusion Engineering Design 87 (2012) 603-607.

[5] C. Gleason-González et al., Fusion Engineering Design 109-111 (2016) 693-699.

[6] Chr. Day et al., Proceedings of the 26th IAEA

author's email: Xueli.Luo@kit.edu

Fusion Energy Conference, Kyoto, Japan (2016) FIP/P4-42.
[7] G. Giruzzi et al., Nuclear Fusion 57 (2017) 085001
[8] Saksaganskii, Molecular flow in complex vacuum systems, G.L. Gordon and Breach Science Publishers, New York, 1988.
[9] B. Spears, JT-60SA Plant Integration Document (PID) V3.8 (May 2015)
[10] V.B. Yuferov et al, Sov.Phys.Tech.Phys., 14 (1970)1261.
[11] J.H. Kamperschroer et al., J. Vac. Sci. Technol. A 8 (1990) 3079-3083
[12] A. Mack et al., Experimental investigations of helium cryotrapping by argon frost, Proc. 4th Topical Meeting on Tritium Technology in Fission, Fusion and Isotopic Applications, Sept. 1991, Albuquerque, NM, USA.
[13] M. Scannapiego, C. Day, and V. Hauer, Fusion Engineering Design 89 (2014) 2446-2450.
[14] H. Suzuki and S. Sakurai, Pumping Speed and Heat Load of the Cryopanel for the JT-60SA Divertor from Conceptual design, technical report.
[15] P.C. Souers, Hydrogen Properties for Fusion Energy, University of California Press, Berkley, CA, USA, 1986.
[16] CRYODATA, http://www.htess.com/software.htm
[17] V.A. Rabinovich, A.A. Vasserman, V.I. Nedostup, L.S. Veksler, Thermophysical Properties of Neon, Argon, Krypton, and Xenon, Hemisphere Publishing Corporation, Washington, USA, 1988.

author's email: Xueli.Luo@kit.edu